Chemistry Europe
European Chemical Societies Publishing

WILEY VCH

Excellence in Chemistry Research

Announcing our new flagship journal

- Gold Open Access
- Publishing charges waived
- Preprints welcome
- Edited by active scientists

Meet the Editors of *ChemistryEurope*

Luisa De Cola
Università degli Studi di Milano Statale, Italy

Ive Hermans
University of Wisconsin-Madison, USA

Ken Tanaka
Tokyo Institute of Technology, Japan

ChemCatChem

Research Article
doi.org/10.1002/cctc.202300740

Chemistry Europe
European Chemical Societies Publishing

www.chemcatchem.org

Selective Dehydrogenation of Formic Acid Catalyzed by Air-Stable Cuboidal PN Molybdenum Sulfide Clusters

María Gutiérrez-Blanco,[a] Carolin A. M. Stein,[b] Carmina Alfonso,[a] Eva Guillamón,[a] Vicent S. Safont,[a] Iván Sorribes,[a, c] Henrik Junge,[b] Matthias Beller,*[b] and Rosa Llusar*[a]

Formic acid is considered as a promising hydrogen storage material in the context of a green hydrogen economy. In this work, we present a series of aminophosphino and imidazolylamino Mo_3S_4 cuboidal clusters which are active and selective for formic acid dehydrogenation (FAD). Best results are obtained with the new $[Mo_3S_4Cl_3(ed^ip_rp)_3](BPh_4)$ (**4**(BPh_4)) (ed^ip_rp = (2-(diisopropylphosphino)ethylamine)) cluster, which is prepared through a simple ligand exchange process from the $Mo_3S_4Cl_4(PPh_3)_3(H_2O)_2$ precursor. Under the conditions investigated, complex **4**$^+$ showed significantly improved performance (TOF = 4048 h^{-1} and 3743 h^{-1} at 120 °C in propylene carbonate using N,N-dimethyloctylamine as base after 10 min and 15 min, respectively) compared to the other reported molybdenum compounds. Mechanistic investigations based on stoichiometric and catalytic experiments show that cluster **4**$^+$ reacts with formic acid in the presence of a base to form formate substituted species $[Mo_3S_4Cl_{3-x}(OCOH)_x(ed^ip_rp)_3]^+$ (x = 1–3) from which the catalytic cycle starts. Subsequently, formate decarboxylation of the partially substituted $[Mo_3S_4Cl_{3-x}(OCOH)_x(ed^ip_rp)_3]^+$ (x = 1, 2, 3) catalyst through a β-hydride transfer to the metal generates the trinuclear Mo_3S_4 cluster hydride. Dehydrogenation takes place through protonation by HCOOH to form Mo–H···HCOOH dihydrogen adducts, with regeneration of the Mo_3S_4 formate cluster. This proposal has been validated by DFT calculations.

Introduction

Major worldwide transformations are required to achieve the United Nations sustainable development goals on affordable and clean energy.[1–3] In this context, hydrogen has emerged as a promising option as a green energy carrier due to its straightforward availability from renewable energy and H_2O.[4] However, specifically storage and transportation of hydrogen remain critical issues regarding safety and practicability. To overcome these limitations, a variety of physical and chemical hydrogen storage materials are currently under investigation.[5] Among them, formic acid (FA) is widely explored due to its chemical properties such as availability, low toxicity and its recyclability *via* CO_2 hydrogenation.[6]

In general, FA decomposition can proceed *via* decarboxylation giving H_2 and CO_2 or by decarbonylation giving H_2O and CO. In addition, FA can disproportionate to afford CH_3OH, H_2O and CO_2. For practical applications, formation of CO should be avoided because it poisons the catalysts in potential follow up fuel cell applications.[7] In the past decade, a variety of suitable homogeneous and heterogeneous catalysts for FA dehydrogenation have been developed.[6,8] Many of the highly selective catalysts are homogeneous organometallic complexes based on precious metals such as Ru,[9] Ir[10,11] or Rh.[12] In recent years, many efforts have been devoted to develop their earth-abundant counterparts and remarkable advances have been achieved, e.g. using hydrido Fe-PN^{H}P pincer complexes[13] while promising results were also obtained with Mn,[14] Co,[15] or Cu.[16] In most cases, the structure of the ligand has a strong influence on the dehydrogenation activity due to metal-ligand cooperativity which causes stabilization of the active species or assists outer sphere interactions involved in key determining mechanism steps.[17]

While molybdenum is one of the nature's favorite metals for many biological transformations, when it comes to CO_2 hydrogenation or FA dehydrogenation, the number of reported Mo-based catalysts for FA decomposition is still rare. In fact, only a few heterogeneous Mo-based catalysts (carbides, nitrides and/or sulfides) are known to catalyze the dehydrogenation of formic acid.[18–23] However, in these cases the chemoselectivity remains a key issue due to the generation of CO. As an example, utilizing MoS_2 nanoclusters deposited on graphene surfaces

[a] M. Gutiérrez-Blanco, Dr. C. Alfonso, Dr. E. Guillamón, Prof. Dr. V. S. Safont, Prof. Dr. I. Sorribes, Prof. Dr. R. Llusar
Departament de Química Física i Analítica
Universitat Jaume I
Av. Sos Baynat s/n 12071 Castelló (Spain)
E-mail: rosa.llusar@uji.es

[b] C. A. M. Stein, Dr. H. Junge, Prof. Dr. M. Beller
Leibniz-Institut für Katalyse e.V.
Albert-Einstein-Street 29a, 18059 Rostock (Germany)
E-mail: Matthias.Beller@catalysis.de
Homepage: http://www.catalysis.de/en/research/applied-homogeneous-catalysis

[c] Prof. Dr. I. Sorribes
Current Address:
Institute of Advanced Materials (INAM)
Universitat Jaume I
Av. Sos Baynat s/n, 12071 Castelló (Spain)

Supporting information for this article is available on the WWW under https://doi.org/10.1002/cctc.202300740

allowed for quantitative conversion of FA at 250 °C.[21] The major decomposition products are CO_2, H_2 and methyl formate (MF); therefore, in this case disproportionation competes with FA dehydrogenation. Simulation studies of the nanoclusters structure revealed the presence of Mo-edge atoms that the authors tentatively identified as the active sites of the reaction. In 2021, Li and coworkers reported a CO-free FA dehydrogenation protocol using MoS_2 on graphene decorated on Ni foam (Ni/G/MoS_2).[23] Full conversion and 100% selectivity towards H_2 and CO_2 is achieved at 100 °C. Notably, this latter material has a sulfur terminated surface which has strong adsorption for the H sites and weak adsorption for the O sites of FA. According to the authors, this results in the high selectivity of their protocol.

Homogeneous catalytic systems for selective FA dehydrogenations using molybdenum are also limited to a few examples shown in Scheme 1.[24–26] Interestingly, the pincer $(PN^HP)MoH(OCOH)(CO)_2$ compound (Beller and Junge, Scheme 1), in addition to FA dehydrogenation, it also catalyzes its disproportionation to methanol while stoichiometric amounts of methanol are produced in the presence of the mononuclear $Cp^*Mo(PMe_3)_2(CO)H$ hydrido complex (Parkin, Scheme 1). In contrast, the hydrido $[Mo_3S_4H_3(diphosphine)_3]^+$ (Llusar, Scheme 1) cluster catalyst is selective towards H_2 production.

The proposed dehydrogenation reaction mechanism for $Cp^*Mo(PMe_3)_2(CO)H$ and $[Mo_3S_4H_3(diphosphine)_3]^+$ share common features. Both complexes interact with FA to form dihydride $Mo(H_2)$ species or dihydrogen Mo–H···HCOOH species, in the case of $[Mo_3S_4H_3(diphosphine)_3]^+$, from which hydrogen is released with the concomitant formation of formate-substituted derivatives that regenerates the hydrido catalysts through a β-hydride elimination accompanied by CO_2 release. As to $(PN^HP)MoH(OCOH)(CO)_2$, formate decarboxylation through a β-hydride transfer to the metal generates dihydride $Mo(H_2)$ species. Selectivity in favor of either dehydrogenation or decarboxylation is determined in the next step. More specifically, dehydrogenation takes place through dihydrogen reductive elimination or *via* protonation by HCOOH, with regeneration of the $(PN^HP)MoH(OCOH)(CO)_2$ metal hydride. While not mandatory, N–H proton-assisted dehydrogenation may also be operative in this last case. Disproportionation in the presence of mononuclear complexes $Cp^*Mo(PMe_3)_2(CO)H$ and $(PN^HP)MoH(OCOH)(CO)_2$ results from a hydride transfer from the metal dihydride $Mo(H_2)$ species to an activated/protonated molecule of HCOOH. To date, the hydrido $[Mo_3S_4H_3(diphosphine)_3]^+$ cluster is the most active and selective homogeneous Mo-based catalysts for FA dehydrogenation.

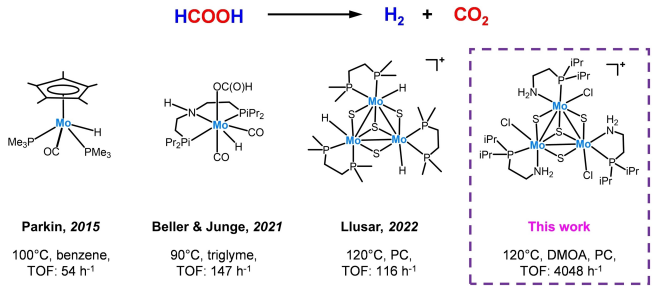

Scheme 1. Reported Mo-based catalysts active in the FA dehydrogenation.

Herein, we report efficient and selective homogeneous molybdenum catalyst for FA dehydrogenation using a trinuclear non-hydride metal cluster sulfide decorated with aminophosphine ligands. The optimal $[Mo_3S_4Cl_3(ed^ip_rp)_3]^+$ (ed^ip_rp = (2-(diisopropylphosphino)ethylamine)) pre-catalyst operates in the presence of a base without fragmentation of the cluster with an activity remarkably higher to that of known homogeneous molybdenum catalysts. The synthesis and crystal structure of this new complex is also presented. Finally, a tentative mechanism for this reaction is postulated based on stoichiometric and catalytic experiments, and validated by theoretical studies.

Results and Discussion

Synthesis and characterization of the catalyst

Motivated by the potential of molybdenum cluster sulfides as FA dehydrogenation catalysts, we undertook an exploratory study aimed to identify active cluster complexes. For that purpose, we tested several trinuclear Mo_3S_4 compounds, represented in Table 1. Except for $\mathbf{4}^+$, the synthesis and crystal structures of the rest of the compounds have been previously reported.[25,27–30] The catalytic tests were performed in a glass reactor connected to a manual burette (Figure SI5). Initial experiments were performed under base-free reaction conditions (120 °C and propylene carbonate (PC) as solvent) employed for the catalytic hydrogen production from FA using the diphosphino $[Mo_3S_4H_3(diphosphine)_3]^+$ ($\mathbf{2}^+$) cluster.[26] As no gas evolution was observed using the Mo_3S_4 catalysts $\mathbf{3}^+$ to $\mathbf{7}^+$, catalytic tests were performed in the presence of Et_3N. In general, the proposed mechanism for FA dehydrogenation using bifunctional ligands proceeds *via* a formate intermediate, therefore, the base is important to start the catalytic cycle.[31]

Two aminophosphino trinuclear complexes ($\mathbf{3}^+$ and $\mathbf{4}^+$) differing in the nature of the group attached to the phosphorous atom and three imidazolyl amino cluster compounds ($\mathbf{5}^+$–$\mathbf{7}^+$) with the NH_2 moiety gradually substituted by methyl groups were investigated in our work.[29,30] Complex **1**, a typical precursor for the preparation of Mo_3S_4 complexes was also tested.[27] For comparative purposes, we have also included in our studies the diphosphino Mo_3S_4 hydrido cluster ($\mathbf{2}^+$) and the pincer complex $(PN^HP)Mo(OCOH)(CO)_2$ (**8**).[25,28] The results of catalyst screening are summarized in Table 1. Gas evolution/time diagrams are represented in Figure SI7. In the case of the already reported diphosphino $[Mo_3S_4H_3(diphosphine)_3]^+$ ($\mathbf{2}^+$) catalyst, addition of Et_3N improved the catalytic activity (TOF 116 vs 411 h^{-1}).[26] For the other Mo_3S_4 clusters ($\mathbf{3}^+$-$\mathbf{7}^+$), gas evolution started after addition of the HCOOH/Et_3N (5:2) mixture to the preheated solution of the catalysts. While similar TON were obtained for compounds $\mathbf{2}^+$, $\mathbf{3}^+$ and $\mathbf{4}^+$ (Table 1, entries 2–4), the highest catalytic activity was achieved using compound $\mathbf{4}^+$ (Table 1, entry 4). Therefore, replacing the phenyl

Table 1. Catalyst screening for the FA dehydrogenation.[a]

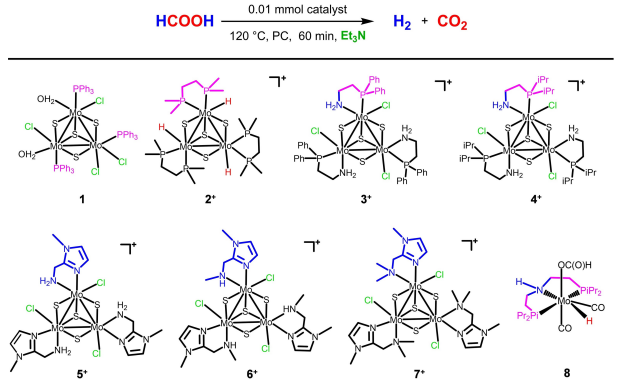

Entry	Catalyst	Conversion(%)[c]	TON[d]	TOF_{10min}[e]
1	**1**	25	25	55
2	**2**$^+$	>99	98	411
3	**3**$^+$	97.5	96	272
4	**4**$^+$	>99	98	589
5	**5**$^+$	85	84	117
6	**6**$^+$	10	10	18
7	**7**$^+$	4	4	18
8	**8**$^+$	2	2	18
9[b]	**4**$^+$	–	–	–

[a] Reaction conditions: HCOOH (1 mmol), Et_3N (0.4 mmol), Mo_3S_4 catalyst (0.01 mmol), PC (1.5 mL), T(120 °C), 60 min. [b] Same conditions as [a] without addition of a base [c] Based on gas evolved. [d] TON values are calculated at the end of the reaction. [e] TOF is obtained for the most active 10 min period of the reaction. Gas evolution monitored with manual burettes, corrected by the blank volume and content of the gas phase analyzed by gas chromatography (GC). The CO content was below the detection limit (<10 ppm) (Figure SI6). Experiments were performed at least twice except entry 2.

group bound to the phosphorous atom of the aminophosphino ligand by isopropyl increased the catalytic activity of the Mo_3S_4 cluster complex. As expected, no catalytic activity was found for **4**$^+$ in the absence of a base (Table 1, entry 9). Little gas evolution was observed for the cluster precursor **1** corroborating the crucial role of the ligand.

The catalytic activity of the imidazolyl amino-containing clusters decreased in the order **5**$^+$ > **6**$^+$ > **7**$^+$ (Table 1, entries 5–7). Hence, we conclude that methylation of one hydrogen atom of the N–H moiety in **5**$^+$ leads to a significant decrease in the catalytic activity. In agreement with this observation, complete alkylation of the N–H moieties in **5**$^+$ drastically lowered the hydrogen yield. To obtain evidence about the cluster integrity during the catalytic protocol, ESI-MS was recorded after catalytic gas evolution in the presence of the **4**$^+$ cation. Notably, no decomposition products could be observed, and the only peak registered corresponds to the **4**$^+$ complex supporting a cluster catalysis mechanism (Figure SI14). The catalytic activity of the mononuclear pincer Mo catalyst (**8**) reported as active by some of us for FA dehydrogenation and disproportionation was also tested under these conditions showing only a negligible activity. In all experiments, the possibility of FA disproportionation was also investigated but neither methanol nor methyl formate were detected by gas chromatography.

For the synthesis of the new cluster cation $[Mo_3S_4Cl_3(ed^ip_rp)_3]^+$ (**4**$^+$), we followed the procedure developed by one of our groups for the synthesis of other Mo_3S_4 derivatives[30,32] The cluster precursor $Mo_3S_4Cl_4(PPh_3)_3(H_2O)_2$ was reacted with a slight excess of the aminophosphine ed^ip_rp ligand in EtOH at room temperature for 3 hours. The reaction proceeds with color changes from green to brown and back to green. The desired product was precipitated with pentane as the chloride salt, redissolved in methanol and precipitated with sodium tetraphenylborate as $[Mo_3S_4Cl_3(ed^ip_rp)_3]BPh_4$ (**4**(BPh_4)). The product identity was confirmed by ESI-MS on the basis of its m/z value of 1005.9 and its characteristic isotopic pattern (Figure SI4).

The structure of cation **4**$^+$ has been determined by single crystal X-ray diffraction as its chloride salt and solved in space group P-1. Figure 1 shows the ORTEP view of **4**$^+$ together with the most relevant bond distances. The crystal structure contains two crystallographically independent cluster units, two chloride atoms and one dichloromethane molecule. The trinuclear Mo_3S_4 unit possesses an incomplete cubane-type arrangement with the molybdenum and sulfur atoms occupying adjacent vertices leaving a vacant metal position. The three metal atoms define an approximately equilateral triangle and the Mo–Mo bond distance of 2.760[6] Å corresponds to a single metal-metal bond. Cluster **4**$^+$ shares main geometric features with other trinuclear cluster analogs.[29]

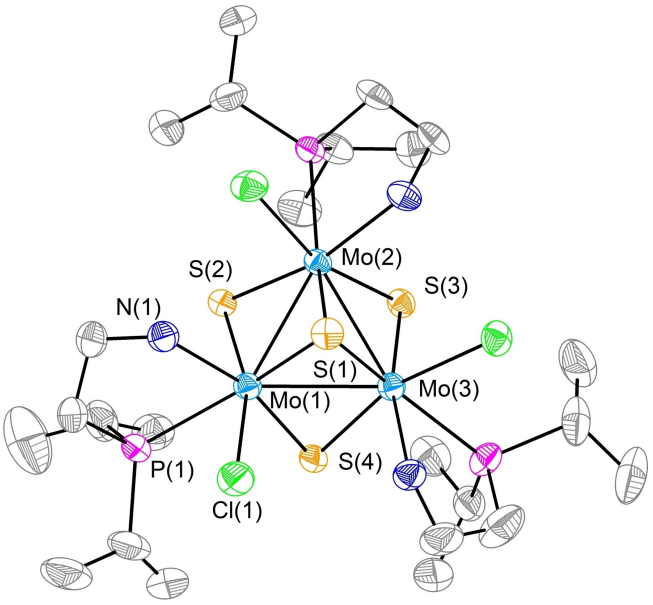

Figure 1. ORTEP representation of the $[Mo_3S_4Cl_3(ed^ip_rp)_3]^+$ (**4**$^+$) cation (ellipsoids at 50 % probability) with the atom-numbering scheme. Hydrogen atoms have been omitted for clarity. Main bond distances: Mo–Mo = 2.760[6] Å, Mo–S(1) = 2.346[4] Å, Mo–$S_{(trans\text{-}NH_2)}$ = 2.300[5] Å, Mo–$S_{(trans\text{-}Cl)}$ = 2.296[6] Å, Mo–Cl = 2.510[12] Å, Mo–N = 2.254[7] Å, Mo–P = 2.576[10] Å. Standard deviations for averaged values are given in square brackets. CCDC 2261460.

Each metal atom in $\mathbf{4}^+$ shows a pseudo-octahedral environment and its coordination sphere includes a phosphorous and a nitrogen atom from the ed^{i}p$_r$p ligand, a chlorine atom, one capping and two bridging sulfur atoms. A relevant feature for this compound is the specific coordination of the aminophosphino ligand in which the three phosphorous atoms are located *trans* to the capping sulfur atom as observed for other aminophosphino M_3S_4 (M = Mo, W) clusters.[29,33]

The solid-state structure of complex $\mathbf{4}^+$ is preserved in solution as evidenced by the $^{31}P\{^1H\}$ NMR spectrum registered in CD_2Cl_2, which showed a single signal at 53.55 ppm attributed to the three equivalent phosphorous atoms from the aminophosphine ligands which are located above the metal plane (Figure SI1). The cluster C_3 symmetry is evidenced by ^1H NMR spectroscopy where the aminophosphine signals demonstrate that all bidentate ligands are equivalent. In particular, the protons associated to the N–H moiety of the ligand appear at 2.80 and 3.29 ppm in agreement with two different hydrogen orientations. More details about ^1H NMR and ^{13}C NMR spectra are given in the Supporting Information (Figures SI2 and SI3).

Catalytic performances

At this point, different important reaction variables were varied such as FA concentration and catalyst loading, solvent, base and FA to base ratio employing $[Mo_3S_4Cl_3(ed^ip_rp)_3]BPh_4$ ($\mathbf{4}(BPh_4)$) as catalyst. The influence of the FA concentration was evaluated keeping the amount of catalyst $\mathbf{4}^+$ constant (Figure SI8 and entries 1–3, Table 2). Increasing the amount of formic acid from 1 to 10 mmol (entries 1–3, Table 2) proportionally increased the TON. Interestingly, the diphosphino $[Mo_3S_4H_3(diphosphine)_3]^+$ ($\mathbf{2}^+$) losses efficiency at higher HCOOH loading that is at lower pH.[26] However, the TOF_{10min} numbers using $\mathbf{4}^+$ decreased on going from 5 to 10 mmol of FA (entries 2–3, Table 2). This is likely due to pH changes over the course of the reaction. A variation of the FA concentration by increasing the solvent volume (Figure SI9 and entries 3–4, Table 2) resulted in a remarkable improvement of the catalytic activity. Next, the catalyst loading was investigated at constant FA concentration (entries 4–6, Figure SI10). A decrease in the catalyst loading by half decreases the catalytic activity; however, doubling the amount of pre-catalyst caused only a *ca.* 2 fold increase of the TOF. Then, we decided to continue our studies using a catalyst concentration of 0.01%, that is, the conditions of entry 4 in Table 2.

Table 2. Molybdenum-catalyzed dehydrogenation of formic acid: Influence of the formic acid concentration and catalyst loading.[a]

Entry	FA (mmol)	Cat. (μmol)	V_{PC} (mL)	$V_{H_2+CO_2}$ (mL)[c]	TON[d]	TOF_{10min} (h^{-1})[f]
1	1	10	1.5	48	98	1472 [g]
2	5	10	1.5	281	574	791
3	10	10	1.5	408	834	288
4[b]	10	10	5	450	921	546
5[b]	10	5	5	305	1247[e]	368
6[b]	10	20	5	482	493	1251

[a] Reaction conditions: catalyst $\mathbf{4}^+$ (0.01 mmol), PC (1.5 mL), T(120 °C). [b] HCOOH (10 mmol), Et_3N (4 mmol), catalyst $\mathbf{4}^+$ (0.01 mmol), PC (5 mL), T(120 °C) [c] Gas evolution monitored with manual burettes, corrected by the blank volume and content of the gas phase analyzed by gas chromatography (GC). [d] TON values are calculated at the end of the reaction. [e] TON value is calculated after system saturation (t = 240 min). [f] TOF values are calculated at the first 10 min of reaction [g] TOF value is calculated after 4 min. All the experiments were performed at least twice, and average values are used in the table. (St. Dev. < 10%)

Previous studies demonstrated that the solvent has a decisive influence in this transformation as it can shift FA decomposition from dehydrogenation to disproportionation.[25] Hence, the effect of the solvent on the reaction was examined and the resulting gas evolution curves are represented in Figure 2a. Significant catalytic activity towards hydrogen evolution was observed in toluene although PC continues to be a better choice. In the case of THF, gas release was almost negligible. The reaction mixture was analysed to detect any potential products resulting from FA disproportionation but neither methyl formate nor methanol were detected. Then, the influence of the temperature was investigated using PC as solvent (Figure 2b). As expected, decreasing the temperature resulted in slower gas evolution. Both gas evolution/time curves in Figure 2a–2b show a slope change in the curve, that is an induction period, which is more visible for the systems with slower kinetics. In the early stage of the reaction, we also observed a color change from green to brown. These observations agree with $\mathbf{4}(BPh_4)$ being the pre-catalyst from which active species are formed after HCOOH/Et_3N addition. Incidentally, $\mathbf{4}(BPh_4)$ does not react with HCOOH in the absence of a base (Figures SI15–SI16).

In the next step, we investigated the influence of the base as well as the FA to base ratio and the results are summarized in Figures 2c–2d. The corresponding gas evolution/time curves are given in the SI (Figures SI11–SI12). The use of N,N-dimethyloctylamine (DMOA) instead of Et_3N (Figure 2c) noticeably increased the performance achieving TOFs of *ca.* 2000 h^{-1}. Decrease of the FA to DMOA ratio (Figure 2d) to 11:10 resulted in a significant improvement of the catalytic activity reaching TOFs of 4048 h^{-1} (3743 h^{-1} after 15 min). On the other hand, a significant drop in the catalytic activity was found upon increasing the FA to DMOA ratio from 5:2 to 5:1 (TOF: 1736 *vs.* 374 h^{-1}) which demonstrates the crucial role of the base during the reaction.

Finally, recycling experiments were performed. After each run, as the base is expected to be recovered, only neat formic acid was added to the solution. The catalyst system stayed active in the tested four runs; however, some loss of activity is observed after the second run as shown in Figure SI13. We assume catalyst deactivation occurs through fragmentation of the trinuclear cluster catalyst, in agreement with the previously described diphosphino Mo_3S_4 cluster catalyst.[26] Hence, to further improve this class of catalysts to a practically applicable level, it is important to increase the stability of the cluster by respective ligand design.

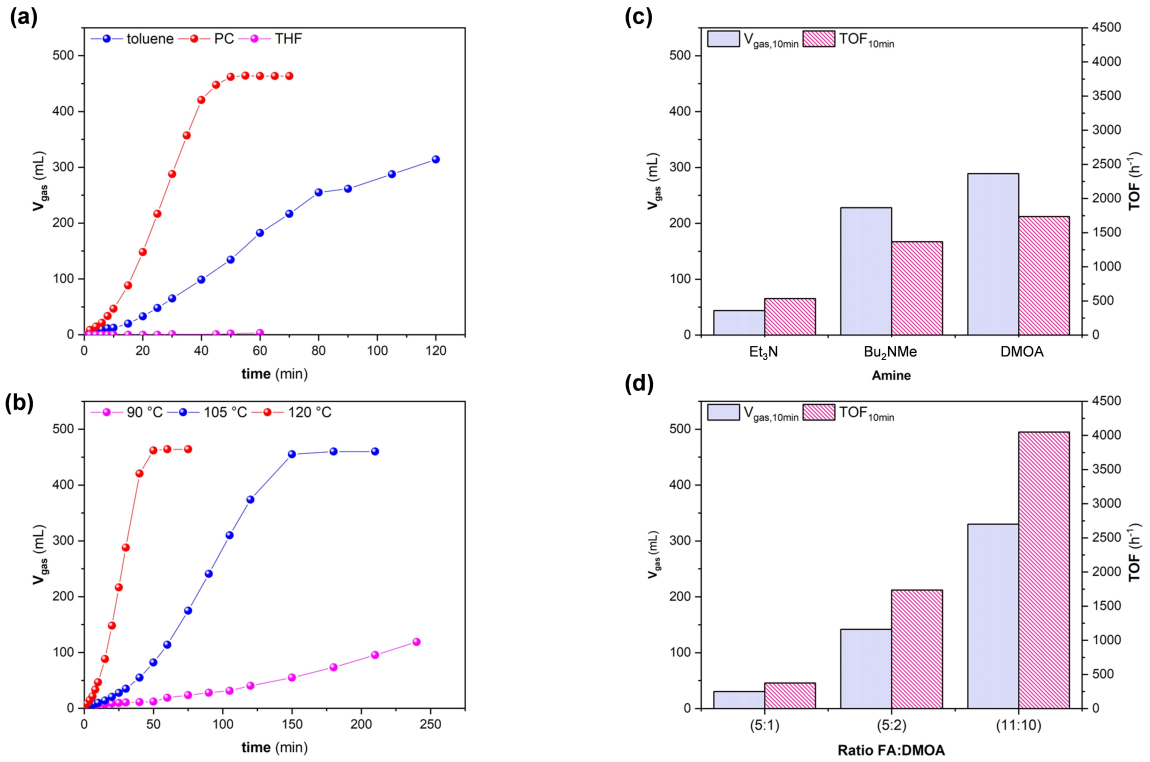

Figure 2. Molybdenum-catalyzed dehydrogenation of formic acid. Influence of (a) solvent (toluene, PC, THF), (b) temperature (90 °C, 105 °C, 120 °C), (c) base (Et_3N, Bu_2NMe, DMOA) and (d) ratio of FA:DMOA (5:1,5:2,11:10). TOF values are obtained for the first active 10 min period of the reaction. Standard conditions if not otherwise noted: $\mathbf{4}^+$ was used as the catalyst, 10 mmol of FA, 4 mmol Et_3N, T = 120 °C, 5 mL PC.

Mechanistic insights

Previous studies have shown that aminophosphino $[M_3S_4X_3(aminophosphine)_3]^+$ (M=Mo, W) cluster complexes present distinctive features when compared to its diphosphine analogs such as the facile substitution of the halide ligands (X) by other halides or pseudohalides. Conversion occurs *via* the formation of two reaction intermediates associated to the mono and disubstituted trinuclear complexes.[34] Kinetic studies showed that the mechanism of substitution is strongly dependent on the nature of the leaving group. On the other hand, Collision Induced Dissociation (CID) experiments combined with the calculated energy requirements for the partial decoordination of the ligand are contrary to the general idea regarding the hemilabile character of the aminophosphine ligand.[29]

For FA dehydrogenation reactions it is generally accepted that the corresponding formate complex is the starting point or crucial intermediate of the catalytic cycle. Hence, the presence of base and pH are important factors for this transformation.[17,24,26,31] From the formate species, β-hydride elimination produces the respective hydride complex. To gain insight on the ligand substitution process, halide by formate, we investigated the stoichiometric reaction between $\mathbf{4}^+$ and formic acid in presence of Et_3N using a FA:Et_3N (5:2) mixture. Milder reaction conditions (lower temperature) compared to those of the catalytic protocol were employed to prevent complications due to β-hydride elimination. The $^{31}P\{^1H\}$ NMR spectrum of the mixture after 10 minutes of reaction in acetonitrile-d_3 (CD_3CN) at 50 °C shows a series of signals with the typical pattern of a sequential substitution of the $\mathbf{4}^+$ chlorine atoms by formate ligands, represented in Figure 3a.[26] It should be noted that the loss of symmetry of the two resulting intermediates the monosubstituted $[Mo_3S_4Cl_2(OCOOH)(ed^ip_rp)_3]^+$ (**M**) and disubstituted $[Mo_3S_4Cl(OCOOH)_2(ed^ip_rp)_3]^+$ (**D**) makes the three phosphorus atoms non-equivalent. For both cluster complexes, three signals of equal intensity are expected in the $^{31}P\{^1H\}$ NMR spectrum. The singlet observed at δ = 56.70 ppm has been tentatively assigned to the triple substituted $[Mo_3S_4(OCOOH)_3(ed^ip_rp)_3]^+$ product (**T**) which recovers the C_3 symmetry of its $\mathbf{4}^+$ cluster precursor.

To our delight, some crystals were formed overnight in the NMR tube by slow evaporation of the solvent. While the quality of most of these crystals was not suitable for single crystal X-ray diffraction experiments, finally we were able to select one crystal valid for that purpose. Figure 3b shows the ORTEP view of $[Mo_3S_4Cl(OCOH)_2(ed^ip_rp)_3]^+$ (**D**) together with the most relevant bond distances. The crystal structure is solved in space group P-1 and it contains one crystallographically independent cluster unit of formula $[Mo_3S_4Cl(OCOH)_2(ed^ip_rp)_3]^+$ resulting from the substitution of two of the chlorine atoms bound to molybdenum in $\mathbf{4}^+$ by two formate ligands. Incidentally, one of the ed^ip_rp ligand is disordered over two positions (see Experimental Section).

The $[Mo_3S_4Cl(OCOH)_2(ed^ip_rp)_3]^+$ cation shares common structural features with its chloride cluster precursor $\mathbf{4}^+$. Inspection of the interatomic distances revealed the presence

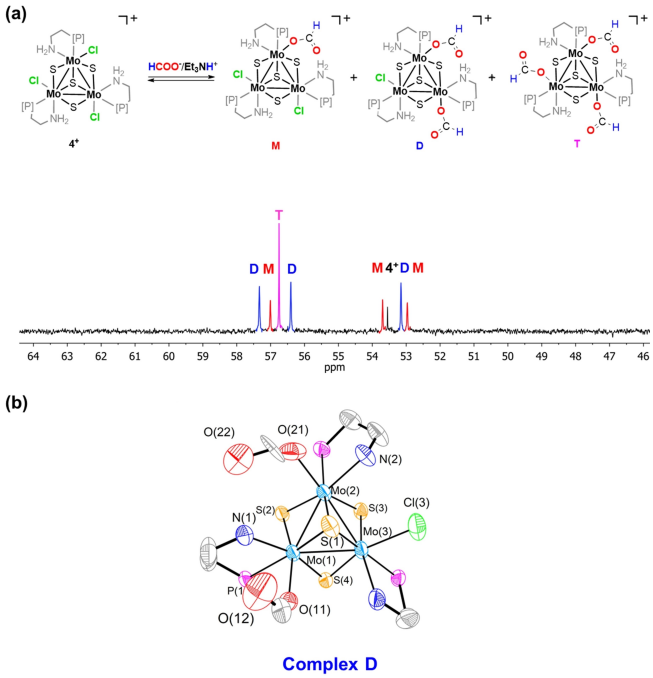

Figure 3. Reaction product between $\mathbf{4}^{+}$ and 7.5 equivalents of a FA/Et_3N(5:2) mixture at 50 °C in CD_3CN. (a) $^{31}P\{^1H\}$ NMR (162 MHz, CD_3CN) spectrum of the reaction mixture, recorded at room temperature. Signals have been tentatively assigned according to the shift in comparison with $\mathbf{4}^{+}$ and the trisubstituted complex (**T**). (b) ORTEP representation of the $[Mo_3S_4Cl(OCOH)_2(ed^ip_rp)_3]^+$ cation (ellipsoids at 50% probability) with the atom-numbering scheme. Hydrogen atoms, isopropyl substituents, and the minor component of the disordered ed^ip_rp ligand have been omitted for clarity. Main bond distances: Mo–Mo = 2.760[5] Å, Mo–S(1) = 2.357[13] Å, $Mo–S_{(trans\text{-}NH_2)}$ = 2.295[12] Å, $Mo–S_{(trans\text{-}Cl)}$ = 2.292 Å, $Mo–S_{(trans\text{-}O)}$ = 2.288 [12] Å, Mo–N = 2.266[4] Å, Mo–P = 2.572[10] Å, Mo–O = 2.244[5] Å, Mo–Cl = 2.512[15] Å. Standard deviations for averaged values are given in square brackets. CCDC 2261461.

of (NH)-H···O(COH) hydrogen bonds with a N(1)–O(11) distance of 2.875 Å and a N(2)–O(21) distance of 2.787 Å. In addition, the terminal formate oxygen atoms O(12) and O(22) forms hydrogen contacts with the H(NH) moiety with a N(1)–O distance of 2.781 Å for O(12) and of 2.805 Å for O(22). In order to prove whether or not the measured crystal was representative of the crystalline sample, we recorded the $^{31}P\{^1H\}$ NMR spectrum of the crystalline product after filtration (Figure SI17). The spectrum shows eight signals of similar intensity associated to $\mathbf{4}^{+}$ and to the mono- (**M**), di- (**D**) and tri-substituted (**T**) formate cluster complexes. Therefore, the crystal structure composition of $[Mo_3S_4Cl(OCOH)_2(ed^ip_rp)_3]^+$ is not representative of the whole crystalline sample. Next, we registered the ESI-MS spectra of the sample at 10 and 20 V (Figures SI18–SI19) The spectrum at 10 V showed one broad signal which can be tentatively assigned to $\mathbf{4}^{+}$ (m/z = 1006) and to the mono-substituted $[Mo_3S_4Cl_2(OCOOH)(ed^ip_rp)_3]^+$ (**M**) (m/z = 1016) complex based on their m/z values and isotopic patterns. Therefore, the di- and tri-substituted species suffer a transformation at the mass spectrometer towards $\mathbf{4}^{+}$ (*vide infra*). At higher cone voltages (20 V), a new signal emerged identified as the hydrido $[Mo_3S_4Cl_2H(ed^ip_rp)_3]^+$ (m/z = 972) cluster cation, which suggests that $[Mo_3S_4Cl_2(OCOH)(ed^ip_rp)_3]^+$ (**M**) undergoes partially a β-hydride elimination at the mass spectrometer to form the corresponding hydrido species.

Based on the above results, we propose a tentative catalytic cycle for FA dehydrogenation, represented in Scheme 2, simplified to a single metal center. In our proposal, the cluster $\mathbf{4}^{+}$ acts as pre-catalyst in agreement with the induction period observed in catalytic reaction monitoring (Figure 2a–2b), as mentioned above. First, the terminal chlorine atoms of the $\mathbf{4}^{+}$ cluster are substituted by $HCOO^-$ ligands to form the formate complex. Next β-hydride elimination followed by CO_2 release leads to the hydrido cluster. In the final step, protonation of the hydride results in the formation of dihydrogen species from which hydrogen is released and the active formate species is regenerated. Protonation of the Mo–H group in cuboidal diphosphino Mo_3S_4 clusters by HCOOH to form dihydrogen Mo–H···HCOOH species is well established.[26,35]

To obtain information about active species and reaction intermediates, the FA dehydrogenation reaction was monitored by ESI mass spectrometry and $^{31}P\{^1H\}$ NMR spectroscopy, represented in Figure 4. For that purpose, milder reaction conditions (1 mmol of FA, 0.030 mmol of Et_3N and 0.010 mmol of the $\mathbf{4}^{+}$ catalyst) were employed to facilitate sampling. At first glance, the reaction monitoring results may seem contradictory. While ESI-MS only showed the presence of cluster $[Mo_3S_4Cl_3(ed^ip_rp)_3]^+$ ($\mathbf{4}^{+}$) without any time evolution along the course of the reaction (Figure 4a); the $^{31}P\{^1H\}$ NMR spectrum evidenced the presence of several species in the reaction mixture (Figure 4b). Since aminophosphino Mo_3S_4 complexes can undergo transformations in the mass spectrometer, the utility of this technique for reaction monitoring is limited except to confirm the operation of a cluster catalysis mechanism. The $^{31}P\{^1H\}$ NMR spectra after 30 minutes of reaction (Figure 4b) within the 52 to 58 ppm range matches with the products obtained from the stoichiometric reaction between the $\mathbf{4}^{+}$ cluster catalyst and formic acid in presence of Et_3N (Figure 3a), that is the mono-, di- and tri-substituted $[Mo_3S_4Cl_{3-x}(OCOH)_x(ed^ip_rp)_3]^+$ (x = 1,2 and 3) species (**M**, **D** and **T**) plus some unreacted $\mathbf{4}^{+}$ cluster. In addition, an extra singlet signal appeared at δ = 64.16 ppm, marked with an **H**. Incidentally, this signal is also observed upon heating the reaction mixture formed by the mono-, di-, and tri-substituted $[Mo_3S_4Cl_{3-x}(OCOH)_x(ed^ip_rp)_3]^+$ (x = 1,2 and 3) species (Figure SI20).

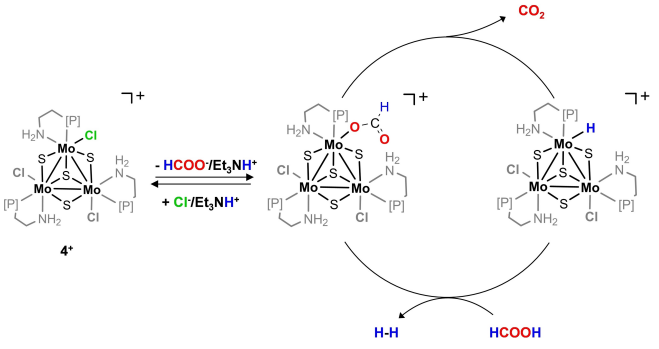

Scheme 2. Proposed catalytic cycle for the dehydrogenation of FA.

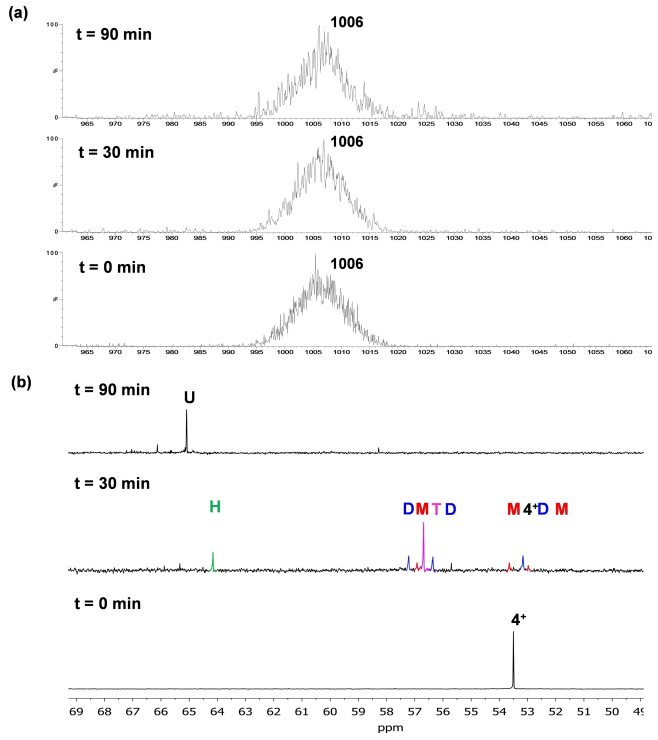

Figure 4. Monitoring of the catalytic reaction by (a) ESI-MS spectrometry and (b) $^{31}P\{^1H\}$ NMR (162 MHz, CD_3CN) spectroscopy. Reaction conditions: HCOOH (1 mmol), Et_3N (0.03 mmol), catalyst $\mathbf{4}^+$ (0.01 mmol), PC (1.5 mL), T (120 °C)

Because it is well known that formate complexes undergo β-hydride elimination to form hydrido species, we have tentatively assigned the singlet signal, labelled as **H**, to the hydrido $[Mo_3S_4H_3(ed^ip_rp)_3]^+$ cluster cation. Notably, we were unable to detect any signal of hydrido species by ^1H NMR spectroscopy. This is not surprising since previous NMR studies on the hydrido $[W_3S_4H_3(edpp)_3]^+$ (edpp = 2-aminoethyl)diphenylphosphine) cluster showed that one of the hydrogen atoms of the NH_2 aminophosphine group is rapidly exchanging with the hydride and as a consequence no hydride signal is seen by ^1H NMR spectroscopy.[36] Unfortunately, all attempts to synthesize and isolate this last postulated species failed.

The $^{31}P\{^1H\}$ NMR spectrum at the end of the reaction when no FA is left (Figure 4b, 90 min) showed a unique signal at $\delta =$ 65.09 ppm labelled as **U**. This signal is also observed upon reacting the $\mathbf{4}^+$ complex catalyst with 40 equiv. of Et_3N at 50 °C (Figure SI21). Previous spectroscopic studies combined with theoretical calculations on the reactivity of the aminophosphino $[W_3S_4Br_3(edpp)_3]^+$ cluster towards Et_3N indicated that the amine acts as a base and abstracts one proton from the NH_2 group of the bidentate ligand while bromine dissociates.[36] Also, Collision Induced Fragmentation (CID) of the $[Mo_3S_4Cl_3(edpp)_3]^+$ ($\mathbf{3}^+$) cluster catalyst occurred with HCl release to yield deprotonated $[Mo_3S_4(edpp\text{-}H)_3]^+$ species.[29] Based on these antecedents, we tentatively assigned the singlet signal at $\delta = 65.09$ ppm to the $[Mo_3S_4(ed^ip_rp\text{-}H)_3]^+$ (**U**) unsaturated Mo=NH amido cluster. It is of interest to remark that the ESI-MS of this reaction mixture, $\mathbf{4}^+$ and Et_3N, showed a sole peak (Figure SI22) attributed to the $\mathbf{4}^+$ cluster catalyst. This fact gives further support to the ability of these aminophosphine Mo_3S_4 clusters to react in the mass spectrometer and transform into the $\mathbf{4}^+$ cluster precursor.

Computational studies

Once direct or indirect experimental evidence were obtained to support our mechanism proposal depicted in Scheme 2, that is formation of the cluster formate and the hydrido complex, we undertook a theoretical DFT study to validate our proposal (see Computational Methods in the SI for details). The calculated free energy profile (Figure 5) has been restricted to a single metal center, a common simplification in this kind of cluster complexes where substitution reactions occur with statistically controlled kinetics.[35] First, complex $\mathbf{4}^+$ exchanges a chlorine atom by a formate ligand generating the active species (**I**). The process is slightly exergonic (-0.76 kcal·mol^{-1}) in agreement with our experimental observation on the coexistence in the reaction mixture of the formate substituted $[Mo_3S_4Cl_{3-x}(OCOH)_x(ed^ip_rp)_3]^+$ (x = 1,2,3) species and the $\mathbf{4}^+$ chloride precursor under stoichiometric conditions. The proposed catalytic cycle (Scheme 2) starts with the active formate complex (**I**). The initial step of the catalytic process entails the liberation of CO_2 from the formate complex (**I**) *via* a β-hydride elimination ($\mathbf{TS_{I\text{-}II}}$). Notice that high temperatures are needed to overcome the barrier (24.9 kcal·mol^{-1}) towards the formation of the hydride species (**II**). This result supports our assignment of the $^{31}P\{^1H\}$ NMR signal registered at $\delta = 64.16$ ppm, labeled with an **H** in Figures 4b and SI20, only observed in the catalytic reaction mixture run at 120 °C or upon heating at 90 °C the $[Mo_3S_4Cl_{3-x}(OCOH)_x(ed^ip_rp)_3]^+$ (x = 0, 1, 2, and 3) reaction mixture prepared under stoichiometric conditions. In the second step, FA addition results in formation of a dihydrogen Mo–H···HCOOH (**III**) adduct with a variation in the free energy of -3 kcal·mol^{-1}. The opposite tendency is observed for the formation of the diphosphino Mo_3S_4 dihydrogen adduct which is endergonic at 120 °C by *ca.* 3 kcal·mol^{-1}.[26,35] We attribute the higher stabilization energy in the case of **III** to the hydrogen bond formation between the carbonyl group of the FA and the NH protons of the ligand in the adjacent metal, with a N···O optimized distance of 2.941 Å. The beneficial role of ligands containing NH functionalities in stabilizing formic acid *via* hydrogen bond interactions has been well established in the literature.[31,37]

In the final step, the dihydrogen adduct (**III**) releases hydrogen through $\mathbf{TS_{III\text{-}I}}$ and regenerates the formate **I** active species. The calculated barrier for the H_2 release (32.2 kcal·mol^{-1}) indicates that dehydrogenation is the rate determining step. Hence, higher temperatures favor this last step of the catalytic cycle and we observe optimum TON upon increasing the reaction temperature to 120 °C. Similar energy barriers were calculated for the FA dehydrogenation using the diphosphino Mo_3S_4 cluster hydride.[26] Overall, FA dehydrogenation is an exergonic process with a relative energy of -11.8 kcal·mol^{-1} that leads to the regeneration of the catalytic active species.

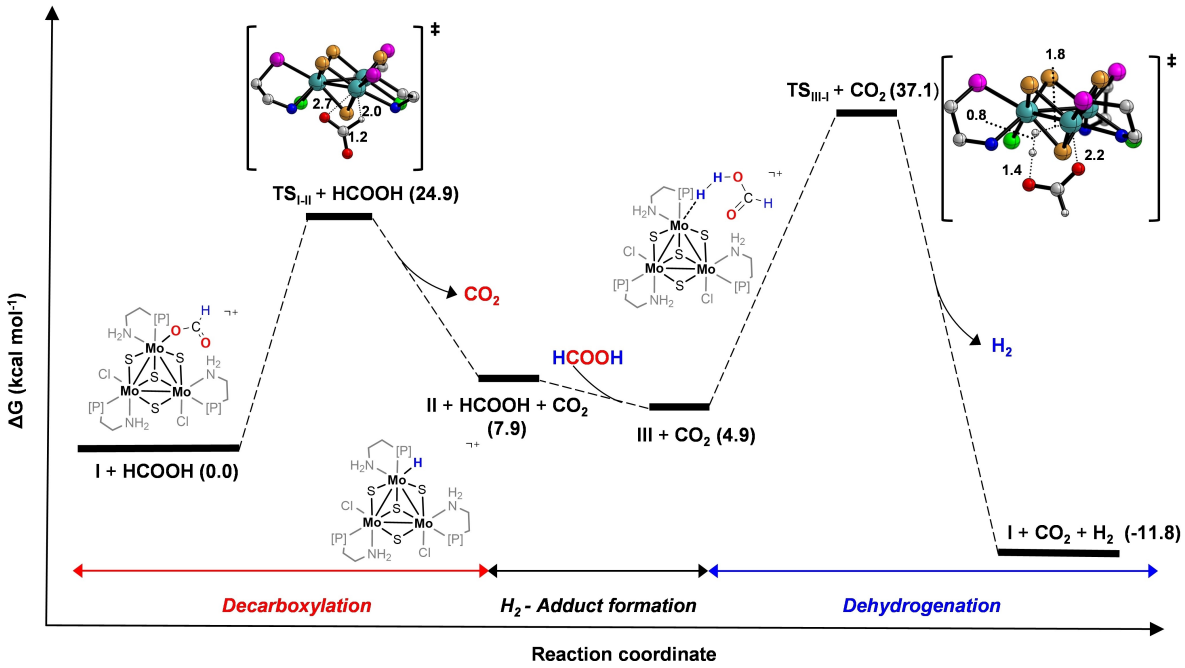

Figure 5. DFT calculated energy profile for FA dehydrogenation catalyzed by $\mathbf{4}^{+}$. Free-energy values are given in kcal mol^{-1}, quoted relative to **I** + HCOOH at 393.15 K and atmospheric pressure. For simplicity, only the skeleton of the ed^{i}p$_{r}$p ligands was drawn. Distances are given in Å. Color code: Mo (cyan), S (orange), P (pink), N (dark blue), O (red), C (grey), H (white).

Conclusions

In this work, we demonstrate that novel molybdenum catalysts are highly active and selective in formic acid dehydrogenation. Within a series of air-stable aminophosphino and imidazolylamino Mo_3S_4 cuboidal clusters, $[Mo_3S_4Cl_3(ed^ip_rp)_3]^+$ ($\mathbf{4}^+$, ed^{i}p$_{r}$p = (2-(diisopropylphosphino)ethylamine)) showed significantly improved performance (TOF = 4048 h^{-1}) compared to all other molybdenum compounds reported for this transformation up to date. In the crystal structure of $\mathbf{4}^+$, the three phosphorous atoms of the ligand are located *trans* to the capping sulfur atoms. Complex $\mathbf{4}^+$ acts as a pre-catalyst from which the active formate substituted species $[Mo_3S_4Cl_{3-x}(OCOH)_x(ed^ip_rp)_3]^+$ (x = 1, 2, 3) are generated.

These last species coexist with the $\mathbf{4}^+$ cluster precursor along the catalytic protocol. The crystal structure of one of the substitution products $[Mo_3S_4Cl(OCOH)_2(ed^ip_rp)_3]^+$ shows hydrogen bonding between the formate hydrogen atoms and the aminophosphine NH_2 protons. A cluster catalysis mechanism is proposed based on stoichiometric and catalytic experiments and our proposal has been validated by DFT calculations. The catalytic cycle entails as the first step elimination of CO_2 starting from the active Mo_3S_4 cluster formate through an intermolecular mechanism without the need of a vacant coordination site. The resulting hydrido cluster interacts with FA to form dihydrogen Mo–H···HCOOH species from which hydrogen is released with the concomitant regeneration of the active formate Mo_3S_4 cluster. The overall process is highly selective with a CO content in the generated gas phase bellow 10 ppm.

Experimental Section

General remarks

All reactions were carried out under inert atmosphere (nitrogen or argon) using standard Schlenck techniques. Reactants obtained from commercial sources were used as received. Solvents were degassed through three freeze-thaw cycles and stored under argon or nitrogen. Elemental analyses were carried out on a EuroEA3000 Eurovector Analyzer. ^{1}H NMR spectra were obtainted at Bruker Avance III HD 400 MHz or 300 MHz. ^{13}C{^{1}H} NMR spectra were obtained at 101 MHz .^{31}P{^{1}H} NMR spectra were recorded at 121 MHz or 162 MHz. NMR chemical shifts are reported in ppm and were referenced to the solvents. ^{31}P NMR chemical shifts are reported in ppm referenced to an external 85 % solution of H_3PO_4. Abbreviations used in the reported NMR experiments: b, broad; s, singlet; d, doublet; t, triplet; m, multiplet. . High resolution mass spectra were registered in a QTOF Premier instrument equipped with an orthogonal Z-spray-electrospray interface (Waters, Manchester, UK) operated in the V-mode at a resolution of ca. 10 000 (FWHM). The drying and cone gas was nitrogen set to flow rates of 300 and 30 L h^{-1}, respectively. A capillary voltage of 3.5 kV was used in the positive scan mode and the cone voltage was set to Uc = 20 V .ESI-mass spectra were registered using a triple quadrupole mass spectrometer with an orthogonal Z-spray electrospray source (Waters, Manchester). The temperature of the source block was set to 100 °C, and the solvation temperature was set to 120 °C. A capillary voltage of 3.3 kV was used in the positive scan mode, and the cone voltage was set to *Uc* = 20 V. Sample solutions in CH_3CN were injected with a syringe pump directly connected to the ESI source at a flow rate of 10 μL min^{-1}. Chemical identification of the cluster species was carried out by comparing the experimental and theoretical isotopic pattern calculated from its elemental composition by using the MassLynx 4.1 program.[38] Gas content was determined by gas-phase GC. Presence of methyl formate or methanol in the reaction mixture were performed in the liquid

phase(s) by GC using hexadecane as internal standard. GC measurements were carried out on an Agilent 6890A GC System equipped with a FID and a capillary column Agilent (HP-innowax, 30 m×250 μm×0.25 μm). Formic acid was quantified in the liquid phase by HPLC (Nucleodur C18 Pyramid 0.25 m, 5 μm, UV (210 nm)) applying propionic acid as internal standard.

Catalyst preparation

All reactions were performed under a nitrogen atmosphere using standard Schlenck techniques. The trinuclear precursor $Mo_3S_4Cl_4(PPh_3)_3(H_2O)_2$ (**1**) was prepared according to the literature procedure.[27] Cluster salts $[Mo_3S_4H_3(dmpe)_3](BPh_4)$ [**2**](BPh$_4$), $[Mo_3S_4Cl_3(edpp)_3]BPh_4$ [**3**](BPh$_4$), $[Mo_3S_4Cl_3(ImNH_2)_3]BF_4$ [**5**](BF$_4$), $[Mo_3S_4Cl_3(ImNHMe)_3]BF_4$, [**6**](BF$_4$) and $[Mo_3S_4Cl_3(ImNMe_2)_3]BF_4$ [**7**]BF$_4$ were obtained following previously reported synthetic methodologies.[28–30] Mononuclear molybdenum catalyst was provided by the group ''Catalysis for Energy Technlogies'' in LIKAT.

Synthesis of $[Mo_3S_4Cl_3(ed^ip_rp)_3](BPh_4)$ [4](BPh$_4$): A small excess of the diisopropylaminophosphine ligand (0.076 g, 0.473 mmol) was added to a green suspension of the freshly prepared $[Mo_3S_4Cl_4(PPh_3)_3(solv)_2]$ cluster (0.200 g, 0.147 mmol) in 40 mL of nitrogen flushed ethanol. This addition was accompanied by color changes (green→brown→green) and caused the complete disolution of the solid. The reaction mixture was reacted for 3 hours at room temperature and then, the volume is reduced to $^1/_4$ of the initial volume in the vacuum line. Following, pentane was added until a precipitate appeared and the mixture was kept in the fridge overnight to complete precipitation process. Next, the solid was separated by filtration, washed with hot hexane and counter anion exchange was carried out by redissolving the solid in the minimum amount of methanol and adding $NaBPh_4$ to the methanolic solution caused the precipitation of the desired green solid. Again, the solid was separated by filtration and washed with methanol and diethyl ether, affording the air-stable product characterized as $[Mo_3S_4Cl_3(ed^ip_rp)_3](BPh_4)$ (0.110 g, 68% yield).

^{1}H NMR (CD_2Cl_2, 400 MHz): δ = 1.17 (dd, J = 15.1 Hz and 7.4 Hz, 9H,CH_3, H_E), 1.26 (dd, J = 14.0 and 7.0 Hz,9H, CH_3, H_E), 1.59–1.67(m, 9 H, CH_3, H_F), 1.70 (dd, J = 15.5 and 7.0 Hz, 9H, CH_3, H_F), 2.32–2.49(m, 6H, CH_2-N, H_B), 2.56 (m, 3H, CH–P, *Hc*), 2.74 (b, 3H, NH, H_A), 3.16 (dp, J = 9.2 and 7.1 Hz, 3H, CH, H_D); 3.32 (d, J = 11.3 Hz, 3H, NH, H_A); 3.37–3.50 (m, 3H, CH–P, H_C), 3.71 (h, J = 7.4 Hz, 3H, CH, H_D);6.87 (t, J = 6.6 Hz, 4H, CH, BPh_4^-),7.03 (t, J = 7.4 Hz, 8H, CH, BPh_4^-),7.29-7.34 (m, 8H, CH, BPh_4^-); ^{13}C {^{1}H} NMR (CD_3CN, 101 MHz): δ = 20.77 (s, CH_3, C_E), 21.39 (s, CH_3, C_E), 21.61(s, CH_3, C_F), 21.96 (s, CH_3, C_F), 27.09 (d, CH_2, C_B), 27.47 (d, CH, C_D), 29.65 (d, CH, C_D), 46.57 (d, CH_2, C_C), 122.28 (s, CH, BPh_4^-), 126.19 (s, CH, BPh_4^-), 136.51 (s, CH, BPh_4^-); ^{31}P{^{1}H} NMR (162 MHz, CD_2Cl_2) δ: 53.55 (s, 3P) ppm; HR-MS (ESI) *m/z* calcd for $Mo_3S_4Cl_3C_{24}H_{60}N_3P_3^+$: 1005.9100 $[M]^+$; found: 1005.8958 Elemental analysis (%) calcd for $Mo_3S_4Cl_3P_3N_3C_{48}H_{80}B$: C. 43.50; H: 6.08; N: 3.17; S: 9.68; found C: 43.95; H: 6.18; N: 3.32; S: 9.79.

X-ray data collection and structure refinement

Single crystals of $[Mo_3S_4Cl_3(ed^ip_rp)_3]Cl$ [**4**]Cl cluster suitable for X ray analysis were obtained by slow diffusion of pentane over a dichloromethane solution containing the cluster. Crystals of $[Mo_3S_4Cl(HCOO)_2(ed^ip_rp)_3]BPh_4$ were grown by slow evaporation of a sample solution of the reaction mixture between $\mathbf{4}^+$ and excess of FA:Et_3N (5:2) in CD_3CN. Diffraction data collection was performed at T = 200(14) K on an Agilent Supernova diffractometer equipped with an Atlas CCD detector. Mo-K_α radiation (λ = 0.71073 Å) was used for cluster $\mathbf{4}^+$ and Cu-K_α radiation (λ = 1.54184 Å) in the case of $[Mo_3S_4Cl(OCOH)_2(ed^ip_rp)_3]^+$. No instrument or crystal instabilities were observed during data collection. Absorption corrections based on the multiscan method were applied.[39,40] The structures were solved by direct methods and refined by the full-matrix method based on F^2 with the program SHELXL-13 using the Olex2 software package.[41–43]

The structures of the complex salts [**4**]Cl·CH_2Cl_2 and $[Mo_3S_4Cl(OCOH)_2(ed^ip_rp)_3]BPh_4\cdot CH_3CN$ were refined in the triclinic $P\bar{1}$ space group. Graphics were performed with the Diamond visual crystal structure information system software.[44] Hydrogen atoms were refined in their geometrically calculated positions using a riding model, whereas those bond to disordered C atoms were not included in the model. The non-hydrogen atoms of the clusters and the counterions were refined anisotropically. In both cases, a solvent molecule was found in the model. In the $\mathbf{4}^+$ complex one of the chloride counter anions was found disordered over two positions with relative occupancies of 0.58 and 0.42. Also, one C atom of the isopropyl ligand was disordered over two positions, C44 and C45, with relative occupancies of 0.5. For $[Mo_3S_4Cl(OCOH)_2(ed^ip_rp)_3]^+$, also one P atom of one of the ed^ip_r ligands was disordered over two positions P28 A and P28B with a chemical occupancy of 0.15 and 0.85. Nor restrains neither constraints were employed during the refinement. One disordered molecule of acetonitrile was modeled using the solvent mask tool (21 electrons detected, 22 electrons assigned to the disordered CH_3CN; solvent r = 1.2; truncation = 1.2)

General procedure for FA dehydrogenation

A 3-neck double wall reactor is attached to a condenser connected to a manual burettes system, illustrated in Figure SI5. The apparatus is purged 3 times and flushed with argon for 15 minutes. Solvent and the catalyst are added under an argon overpressure. The setup is heated to the desired temperature while being flushed with argon. Once the temperature is reached, the burette is closed to the atmosphere and the argon/vacuum line is closed. After letting the system equilibrates for 30–60 min, the mixture formic acid: amine is added into the reactor and the timer turns on. When the reaction is finished, a 5 mL degassed syringe was used to obtain a gas sample analyzed by gas chromatography.

Computational details

DFT calculations were run with Gaussian 09 (Revision D.01).[44] Geometry optimizations were carried out at the BP86/BS1 level,[45,46] where Mo and S atoms were described using the SDD relativistic ECP and associated basis set,[47] with added polarization functions for the latter (ζ = 0.503),[48] and the remaining atoms were described with the 6-31G(d,p) basis set.[49,50] Solvent effects (propylene carbonate, ε = 64.0) were included self-consistently in these optimizations through the PCM method.[51,52] Temperature used was 120 °C and atmospheric pressure. All stationary points were characterized at this level of theory by analytical frequency calculations as either minima (all positive eigenvalues) or transition states (one negative eigenvalue). Intrinsic reaction coordinate (IRC) calculations and subsequent geometry optimizations were used to confirm the minima linked by each transition state. In addition, single-point dispersion corrections were computed using Grimme's D3 parameter set and zero damping.[53] Thus, the free energies shown herein were obtained by adding the dispersion correction to the Gibbs energies computed at the BP86/BS1(PCM) level.

CCDC

Deposition Number(s) CCDC 2261460 (**4**), CCDC 2261461 (D) contains the supplementary crystallographic data for this paper. These data are provided free of charge by the joint Cambridge Crystallographic Data Centre and Fachinformationszentrum Karlsruhe Access Structures service.

Supporting Information

Details on characterization spectra of $[Mo_3S_4Cl_3(ed^ip_rp)_3](BPh_4)$ cluster, crystallographic data, additional information on catalytic and mechanistic experiments and theoretical details including Cartesian coordinates for all optimized systems were provided in the Supporting Information.

Acknowledgements

The financial support of the Spanish Ministerio de Economía y Competitividad (PID2019-107006GB-C22), Generalitat Valenciana (Grant CIAICO/2021/122) and Universitat Jaume I (UJI-B2021-29 and UJI-B2022-56) is gratefully acknowledged. The authors also thank the Serveis Centrals d'Instrumentació Científica (SCIC) of the Universitat Jaume I for providing us with materials characterization facilities and computational resources. Furthermore, we thank Leibniz-Institute for Catalysis for the facilities. C.S., M.B., and H.J. acknowledge financial support from the State of Mecklenburg and Western Pomerania as well as European Union (EFRE, project "h2cycle"). M.G.B thanks the Spanish Ministerio de Economía y Competitividad for a predoctoral fellowship (PRE2019-088511).

Conflict of Interests

There are no conflicts of interest to declare.

Data Availability Statement

The data that support the findings of this study are available in the supplementary material of this article.

Keywords: dehydrogenation · formic acid · homogeneous catalysis · hydrogen · molybdenum sulfide

[1] D. Mellmann, P. Sponholz, H. Junge, M. Beller, *Chem. Soc. Rev.* **2016**, *45*, 3954–3988.
[2] G. W. Huber, S. Iborra, A. Corma, *Chem. Rev.* **2006**, *106*, 4044–4098.
[3] United Nations, "Sustainable Development Goals," can be found under https://sdgs.un.org/goals/goal7, n.d.
[4] S. J. Davis, N. S. Lewis, M. Shaner, S. Aggarwal, D. Arent, I. L. Azevedo, S. M. Benson, T. Bradley, J. Brouwer, Y.-M. Chiang, C. T. M. Clack, A. Cohen, S. Doig, J. Edmonds, P. Fennell, C. B. Field, B. Hannegan, B.-M. Hodge, M. I. Hoffert, E. Ingersoll, P. Jaramillo, K. S. Lackner, K. J. Mach, M. Mastrandrea, J. Ogden, P. F. Peterson, D. L. Sanchez, D. Sperling, J. Stagner, J. E. Trancik, C.-J. Yang, K. Caldeira, *Science* **2018**, *360*, DOI 10.1126/science.aas9793.
[5] P. Preuster, C. Papp, P. Wasserscheid, *Acc. Chem. Res.* **2017**, *50*, 74–85.
[6] K. Sordakis, C. Tang, L. K. Vogt, H. Junge, P. J. Dyson, M. Beller, G. Laurenczy, *Chem. Rev.* **2018**, *118*, 372–433.
[7] A. Kumar, S. Semwal, J. Choudhury, *ACS Catal.* **2019**, *9*, 2164–2168.
[8] M. Younas, M. Rezakazemi, M. S. Arbab, J. Shah, W. U. Rehman, *Int. J. Hydrogen Energy* **2022**, *47*, 11694–11724.
[9] S. Kar, M. Rauch, G. Leitus, Y. Ben-David, D. Milstein, *Nat. Catal.* **2021**, *4*, 193–201.
[10] J. H. Barnard, C. Wang, N. G. Berry, J. Xiao, *Chem. Sci.* **2013**, *4*, 1234.
[11] A. Iturmendi, M. Iglesias, J. Munarriz, V. Polo, V. Passarelli, J. J. Pérez-Torrente, L. A. Oro, *Green Chem.* **2018**, *20*, 4875–4879.
[12] P. Hermosilla, A. Urriolabeitia, M. Iglesias, V. Polo, M. A. Casado, *Inorg. Chem. Front.* **2022**, *9*, 4538–4547.
[13] E. A. Bielinski, P. O. Lagaditis, Y. Zhang, B. Q. Mercado, C. Würtele, W. H. Bernskoetter, N. Hazari, S. Schneider, *J. Am. Chem. Soc.* **2014**, *136*, 10234–10237.
[14] I. Dutta, N. A. Alobaid, F. L. Menicucci, P. Chakraborty, C. Guan, D. Han, K.-W. Huang, *Int. J. Hydrogen Energy* **2023**, *48*, 26559–26567.
[15] N. Lentz, A. Aloisi, P. Thury, E. Nicolas, T. Cantat, *Organometallics* **2021**, *40*, 565–569.
[16] N. Scotti, R. Psaro, N. Ravasio, F. Zaccheria, *RSC Adv.* **2014**, *4*, 61514–61517.
[17] M. Iglesias, F. J. Fernández-Alvarez, *Catalysts* **2021**, *11*, 1288.
[18] J. Cao, J. Wang, Y. Ma, X. Li, P. Xiaokaiti, X. Hao, A. Abudula, G. Guan, *J. Alloys Compd.* **2018**, *735*, 1463–1471.
[19] J. Wang, X. Li, J. Zheng, J. Cao, X. Hao, Z. Wang, A. Abudula, G. Guan, *Energy Convers. Manage.* **2018**, *164*, 122–131.
[20] Z. Yu, Y. Yang, S. Yang, J. Zheng, X. Hao, G. Wei, H. Bai, A. Abudula, G. Guan, *Appl. Catal. B* **2022**, *313*, 121445.
[21] V. O. Koroteev, D. A. Bulushev, A. L. Chuvilin, A. V. Okotrub, L. G. Bulusheva, *ACS Catal.* **2014**, *4*, 3950–3956.
[22] I. Kurnia, A. Yoshida, Y. A. Situmorang, Y. Kasai, A. Abudula, G. Guan, *ACS Sustainable Chem. Eng.* **2019**, *7*, 8670–8677.
[23] X. Bai, S. Li, Y. Zhang, S. Zhu, L. Gao, R. Cong, W. Yu, S. Wang, B. Liang, Y. Li, *Green Chem.* **2021**, *23*, 7630–7634.
[24] M. C. Neary, G. Parkin, *Chem. Sci.* **2015**, *6*, 1859–1865.
[25] E. Alberico, T. Leischner, H. Junge, A. Kammer, R. Sang, J. Seifert, W. Baumann, A. Spannenberg, K. Junge, M. Beller, *Chem. Sci.* **2021**, *12*, 13101–13119.
[26] E. Guillamón, I. Sorribes, V. S. Safont, A. G. Algarra, M. J. Fernández-Trujillo, E. Pedrajas, R. Llusar, M. G. Basallote, *Inorg. Chem.* **2022**, *61*, 16730–16739.
[27] V. P. Fedin, M. N. Sokolov, Y. V. Mironov, B. A. Kolesov, S. V. Tkachev, V. Y. Fedorov, *Inorg. Chim. Acta* **1990**, *167*, 39–45.
[28] A. G. Algarra, M. G. Basallote, M. J. Fernández-Trujillo, M. Feliz, E. Guillamón, R. Llusar, I. Sorribes, C. Vicent, *Inorg. Chem.* **2010**, *49*, 5935–5942.
[29] T. F. Beltrán, V. S. Safont, R. Llusar, *Eur. J. Inorg. Chem.* **2016**, *2016*, 5171–5179.
[30] M. Gutiérrez-Blanco, E. Guillamón, V. S. Safont, A. G. Algarra, M. J. Fernández-Trujillo, K. Junge, M. G. Basallote, R. Llusar, M. Beller, *Inorg. Chem. Front.* **2023**, *10*, 1786–1794.
[31] M. Iglesias, L. A. Oro, *Eur. J. Inorg. Chem.* **2018**, 2125–2138.
[32] E. Pedrajas, I. Sorribes, K. Junge, M. Beller, R. Llusar, *ChemCatChem* **2015**, *7*, 2675–2681.
[33] T. F. Beltrán, R. Llusar, *Polyhedron* **2019**, *167*, 39–43.
[34] T. F. Beltrán, J. Á. Pino-Chamorro, M. J. Fernández-Trujillo, V. S. Safont, M. G. Basallote, R. Llusar, *Inorg. Chem.* **2015**, *54*, 607–618.
[35] V. S. Safont, I. Sorribes, J. Andrés, R. Llusar, M. Oliva, M. R. Ryzhikov, *Phys. Chem. Chem. Phys.* **2019**, *21*, 17221–17231.
[36] J. A. Pino-Chamorro, T. F. Beltrán, M. J. Fernández-Trujillo, M. G. Basallote, R. Llusar, A. G. Algarra, *Eur. J. Inorg. Chem.* **2017**, 5006–5014.
[37] A. Luque, A. Iturmendi, L. Rubio-Pérez, J. Munárriz, V. Polo, V. Passarelli, M. Iglesias, L. A. Oro, *J. Organomet. Chem.* **2020**, *916*, 121259.
[38] *MassLynx*, Waters Corporation, Milford, MA, **2005**.
[39] *CrysAlis*, version 171.36.24, Agilent Technologies, Santa Clara, CA, **2012**.
[40] R. C. Clark, J. S. Reid, *Acta Crystallogr. Sect. A* **1995**, *51*, 887–897.
[41] O. V. Dolomanov, L. J. Bourhis, R. J. Gildea, J. A. K. Howard, H. Puschmann, *J. Appl. Crystallogr.* **2009**, *42*, 339–341.
[42] L. J. Bourhis, O. V. Dolomanov, R. J. Gildea, J. A. K. Howard, H. Puschmann, *Acta Cryst* **2015**, *71*, 59–75.
[43] G. M. Sheldrick, *Acta Crystallogr. Sect. A* **2008**, *64*, 112–122.
[44] Gaussian 09. Revision D.01; M. J. Frisch, G. W. Trucks, H. B. Schlegel, G. E. Scuseria, M. A. Robb, J. R. Cheeseman, G. Scalmani, V. Barone, B. Mennucci, G. A. Petersson, H. Nakatsuji, M. Caricato, X. Li. H. P.

Hratchian, A. F. Izmaylov, J. Bloino, G. Zheng, J. L. Sonnenberg, M. Hada, M. Ehara, K. Toyota, R. Fukuda, J. Hasegawa, M. Ishida, T. Nakajima, Y. Honda, O. Kitao, H. Nakai, T. Vreven, J. A. Montgomery, Jr. J. E. Peralta, F. Ogliaro, M. Bearpark, J. J. Heyd, E. Brothers, K. N. Kudin, V. N. Staroverov, T. Keith, R. Kobayashi, J. Normand, K. Raghavachari, A. Rendell, J. C. Burant, S. S. Iyengar, J. Tomasi, M. Cossi, N. Rega, J. M. Millam, M. Klene, J. E. Knox, J. B. Cross, V. Bakken, C. Adamo, J. Jaramillo, R. Gomperts, R. E. Stratmann, O. Yazyev, A. J. Austin, R. Cammi, C. Pomelli, J. W. Ochterski, R. L. Martin, K. Morokuma, V. G. Zakrzewski, G. A. Voth, P. Salvador, J. J. Dannenberg, S. Dapprich, A. D. Daniels, O. Farkas, J. B. Foresman, J. V. Ortiz, J. Cioslowski, D. J. Fox, Gaussian. Inc.: Wallingford CT. **2013**.

[45] J. P. Perdew, *Phys. Rev. B.* **1986**, *33*, 8822–8824.

[46] A. D. Becke, *Phys. Rev. A.* **1988**, *38*, 3098.

[47] D. Andrae, U. Häussermann, M. Dolg, H. Stoll, H. Preuss, *Theor. Chim. Acta.* **1990**, *77*, 123–141.

[48] A. Hollwarth, M. Böhme, S. Dapprich, A. W. Ehlers, A. Gobbi, V. Jonas, K. F. Köhler, R. Stegmann, A. Veldkamp, G. Frenking, *Chem. Phys. Lett.* **1993**, *208*, 237–240.

[49] W. J. Hehre, R. Ditchfield, J. A. Pople, *J. Chem. Phys.* **1972**, *56*, 2257–2261.

[50] P. C. Harihanan, J. A. Pople, *Theor. Chim. Acta.* **1973**, *28*, 213–222.

[51] M. Cossi, G. Scalmani, N. Rega, V. Barone, *J. Chem. Phys.* **2002**, *117*, 43–54.

[52] J. Tomasi, B. Mennucci, R. Cammi, *Chem. Rev.* **2005**, *105*, 2999–3093.

[53] S. Grimme, J. Antony, S. Ehrlich, H. Krieg, *J. Chem. Phys.* **2010**, *132*, 154104.

Manuscript received: June 9, 2023
Revised manuscript received: September 11, 2023
Accepted manuscript online: September 13, 2023
Version of record online: October 2, 2023